On parametric semidefinite programming with unknown boundaries ⋆

Jonathan D. Hauenstein[a,2], Tingting Tang[b]

[a]*Department of Applied and Computational Mathematics and Statistics, University of Notre Dame, 46556 IN, Notre Dame, USA*
[b]*Department of Mathematics and Statistics, San Diego State University, 5500 Campanile Drive, San Diego, 92182 CA,*

Abstract

In this paper, we study parametric semidefinite programs (SDPs) where the solution space of both the primal and dual problems change simultaneously. Given a bounded set, we aim to find the *a priori* unknown maximal permissible perturbation set within it where the semidefinite program problem has a unique optimum and is analytic with respect to the parameters. Our approach reformulates the parametric SDP as a system of partial differential equations (PDEs) where this maximal analytical permissible set (MAPS) is the set on which the system of PDEs is well-posed. A sweeping Euler scheme is developed to approximate this *a priori* unknown perturbation set. We prove local and global error bounds for this second-order sweeping Euler scheme and demonstrate the method in comparison to existing SDP solvers and its performance on several two-parameter and three-parameter SDPs for which the MAPS can be visualized.

Keywords:
Parametric semidefinite programming, numerical algebraic geometry, maximal analytic perturbation set
65H14, 90C22

1. Introduction

The focus of this paper is on parametric semidefinite programming problems (SDPs) where all coefficients of the SDPs depend linearly on multiple parameters. Such parameters are introduced into the SDPs to account for uncertainty about the future, model uncertainty, data errors, and implementation errors as described in Ben-Tal et al. (1998).

Even though parametric linear programming and its sensitivity are extensively studied, there has been much less work on parametric SDPs due its complexity. Most of the work on parametric SDPs focuses on problems with a single parameter that often appears

⋆This article is part of the volume titled "Computational Algebra and Geometry: A special issue in memory and honor of Agnes Szanto".

Email addresses: hauenstein@nd.edu (Jonathan D. Hauenstein), ttang2@sdsu.edu (Tingting Tang)

URL: www.nd.edu/~jhauenst (Jonathan D. Hauenstein)

[1]Agnes Szanto (1966-2022) was a developer and advocate of hybrid symbolic-numeric methods for solving nonlinear problems. In her memory and with great sorrow, we dedicate this paper to our friend, collaborator, and colleague.

[2]This author was supported in part by NSF CCF-1812746, a collaborative project with Agnes Szanto.

only in the coefficients of the objective function or possibly on the the right-hand side of the constrains of the dual problem. The notion of optimal partition from linear program was extended to a single parameter SDP in Goldfarb and Scheinberg (1999). They showed that the set on which the optimal solution is constant under nondegeneracy can be found by another SDP and this set is either a singleton or an open interval. However, these results do not naturally extend to problem with multiple parameters. The optimal set trajectory of time-varying SDPs under the Slater condition (i.e., either the primal or dual is strictly feasible) was classified in Bellon et al. (2021). They showed the optimal solution path has either jump type discontinuity or is piecewise differentiable when there is a nonsingular point on the interval under consideration. These works usually require the problem to be nondegenerate and satisfy the strict complementary condition on the entire parameter set.

Sensitivity analysis of parametric SDPs can be approached with the Jacobian matrix of the corresponding Karush-Kuhn-Tucker (KKT) conditions. There are also some studies investigating the sensitivity analysis of parametric SDPs when this Jacobian is singular. In Sekiguchi and Waki (2021), they examined the sensitivity of a particular parametric SDP which is singular on a given interval. They provided conditions for optimal solution continuity when nondegeneracy fails. It was shown in Miller (1997) that, under certain conditions, the Jacobian matrix can be used to compute the sensitivity of singular parameter SDPs even when primal nondegeneracy fails. Recently, Hauenstein et al. (2022) studied the nonlinearity interval in parametric SDPs and developed a numerical algorithm to compute the nonlinearity interval and transition points on the set where the SDP is feasible. However, all of the studies listed above only consider SDPs with a single perturbation variable except Miller (1997) which only focused on the computation of the sensitivity of optimal solutions at specific values. In this work, we extend the algorithm in Hauenstein et al. (2022) to allow multiple parameters with both perturbations in the objective function as well as on the left and right hand side of the equality constraints simultaneously. We utilize the sensitivity matrix method and partial differential equations (PDEs) constructed by the Davidenko differential equation arising from the primal-dual problem to track the solution of the parametric SDP and approximate the maximal set on which the optimal solution is analytic.

The reminder of this paper is organized as follows. Section 2 formulates the problem using SDPs with Section 3 providing a reformulation using algebraic geometry. This reformulation gives rise to a system of quasilinear PDEs whose well-posedness is investigated in Section 4 and solved using a sweeping Euler scheme in Section 5. Some examples are considered in Section 6. Finally, we summarize our results and discuss the advantages, disadvantages, and future directions to improve the sweeping Euler scheme in Section 7.

2. Problem formulation

The following formulates the parametric semidefinite program under consideration. Uppercase letters are used to represent a matrix or a set. In particular, the identity matrix of size n is represented by I_n or just I if the context is clear. Bold lower cases letters are used represent column vectors, lower case letters (possibly with subscripts) represents scalars, and 0 represents the zero element of the appropriate size in context. In addition, for a matrix $M \in \mathbb{R}^{p\times q}$, we use its lowercase with index m_{ij} to denote the (i,j) entry of M, $M_{\cdot j}$ to denote the j^{th} column of M, and $M_{i\cdot}$ to denote the i^{th} row of M.

Let B be a compact subset of $\mathbb{R}^\ell$. We consider the following primal SDP with affine

perturbation parameter $\boldsymbol{\delta} \in B$:

$$\begin{array}{ll} \text{minimize} & \left(C + \sum_{j=1}^{\ell} \delta_j D_j\right) \bullet X \\ \text{s.t.} & \left(A_i + \sum_{j=1}^{\ell} \delta_j E_{ji}\right) \bullet X = b_i + \sum_{j=1}^{\ell} \delta_j g_{ij}, \quad \text{for } i = 1, \ldots, k \\ & X \succeq 0. \end{array} \tag{1}$$

The dual SDP can be written as follows:

$$\begin{array}{ll} \text{maximize} & (\boldsymbol{b} + \sum_{j=1}^{\ell} \delta_j g_{ij})^T y \\ \text{s.t.} & S = C - \sum_{i=1}^{k} y_i A_i + \sum_{j=1}^{\ell} \delta_j \left(D_j - \sum_{i=1}^{k} y_i E_{ji}\right), \\ & S \succeq 0. \end{array} \tag{2}$$

Let $\mathcal{S}^n$ denote the set of real symmetric $n \times n$ matrices. We assume $C, D_j, A_i, E_{ij} \in \mathcal{S}^n$, $G \in \mathbb{R}^{k \times \ell}$, and $\boldsymbol{b}, \boldsymbol{y} \in \mathbb{R}^k$. For two symmetric matrices $M, N \in \mathcal{S}^n$, the operator $\bullet$ is defined via

$$M \bullet N = \text{trace}(MN)$$

and $M \succeq 0$ denotes that M is a positive semidefinite matrix, i.e., all eigenvalues of M are nonnegative.

The following defines strict complementarity and nondegeneracy of the optimal solution based on Alizadeh et al. (1998).

Definition 1. *Suppose (X, y, S) solves problems (1) and (2).* **Complementary slackness** *holds when $XS = 0$. If $\operatorname{rank} S + \operatorname{rank} X = n$, then* **strict complementarity** *holds. Suppose further that $\operatorname{rank} X = r$ and $\operatorname{rank} S = n - r$. Let $\{w_i\}_1^n$ be the set of eigenvalues of S and $\lambda_1, \ldots, \lambda_r$ be the positive eigenvalues of X. Thus, there is an orthogonal matrix Q such that*

$$X = Q\, Diag(\lambda_1, \ldots, \lambda_r, 0, \ldots, 0)\, Q^T, \qquad S = Q\, Diag(w_1, \ldots, w_n)\, Q^T.$$

Let Q be partitioned as $[Q_1, Q_2]$ where the columns of Q_1 are eigenvectors corresponding to $\lambda_1, \ldots, \lambda_r$. If

$$\begin{pmatrix} Q_1^T A_i Q_1 & Q_1^T A_i Q_2 \\ Q_2^T A_i Q_1 & 0 \end{pmatrix} \qquad \text{for} \quad i = 1, \ldots, k$$

are linearly independent in $\mathcal{S}^n$, then (X, y, S) is **primal nondegenerate**. *Similarly, if $Q_1^T A_i Q_1$ for $i = 1, \ldots, k$ span $\mathcal{S}^r$, then (X, y, S) is* **dual nondegenerate**. *Finally,* **nondegeneracy** *means that (X, y, S) is both primal nondegenerate and dual nondegerate.*

The following are assumed to hold throughout the paper.

Assumption 1. *The compact set $B \subset \mathbb{R}^\ell$ is a semialgebraic set such that 0 is in the interior of B.*

Assumption 2. *The matrices A_i for $i = 1, \ldots, k$ are linearly independent.*

Assumption 3. *At $\boldsymbol{\delta} = 0$, Slater condition, complementary slackness, strict complementarity, and nondegeneracy all hold.*

From Miller (1997), Assumption 2 guarantees the boundedness of the optimal value and Assumption 3 ensures that there is a unique optimal solution without perturbation, i.e., at $\boldsymbol{\delta} = 0$. Let $\hat{X}(\boldsymbol{\delta})$, $\hat{y}(\boldsymbol{\delta})$, and $\hat{S}(\boldsymbol{\delta})$ denote the optimal solution of the prime and dual problems when the optimal solution is unique. Hence, Assumption 3 yields that $\hat{X}(\boldsymbol{\delta})$, $\hat{y}(\boldsymbol{\delta})$, and $\hat{S}(\boldsymbol{\delta})$ are all well-defined and analytic with respect to $\boldsymbol{\delta}$ in a neighborhood of 0.

The goal of this paper is to compute the maximal analytic perturbation set (MAPS).

Definition 2. *The* **maximal analytic perturbation set** *with respect to B is the largest set $U \subset B$ containing 0 in which the following conditions holds for all $\boldsymbol{\delta} \in U$:*

1. *$\boldsymbol{\delta}$ is path-connected to 0 in U,*
2. *there exists a unique primal-dual solution $(\hat{X}(\boldsymbol{\delta}), \hat{y}(\boldsymbol{\delta}), \hat{S}(\boldsymbol{\delta}))$ to (1) and (2) which is analytic (i.e., has a convergent Taylor series expansion) at $\boldsymbol{\delta}$.*

The set U is maximal in that if $W \subset B$ also satisfies the conditions above, then $W \subset U$.

3. Problem reformulation using algebraic geometry

A common technique in semidefinite programming and polynomial optimization is to link the solution with algebraic geometry via the KKT conditions, e.g., see Blekherman et al. (2012). For problem (1) and (2), the first-order KKT conditions are

$$X, S \succeq 0 \tag{3}$$

$$\boldsymbol{F}(X, y, S; \boldsymbol{\delta}) = \begin{pmatrix} (A_i + \sum_{j=1}^{\ell} \delta_j E_{ji}) \bullet X - b_i - \sum_{j=1}^{\ell} \delta_j g_{ij}, \quad \text{for } i = 1, \ldots, k \\ C - \sum_{i=1}^{k} y_i A_i + \sum_{j=1}^{\ell} \left(\delta_j D_j - \sum_{i=1}^{k} y_i E_{ji} \right) - S \\ XS \end{pmatrix} = 0. \tag{4}$$

Let U be the corresponding maximal analytic perturbation set. Then, Item 2 of Def. 2 yields that the KKT conditions are both necessary and sufficient conditions for optimality for $\boldsymbol{\delta} \in U$.

As listed in (4), $\boldsymbol{F}$ is overdetermined. The first two lines in $\boldsymbol{F}$ are naturally symmetric. For the third, namely the complementary slackness condition $XS = 0$, there are different approaches that one can utilize to create a well-constrained polynomial system involving $k + n^2 + n$ polynomials and variables. One approach is to simply take the $(n^2 + n)/2$ equations corresponding to the upper triangular part of XS. Another approach is to take the upper triangular part of a symmetric version of this equation:

$$\frac{1}{2}(SX + XS) = 0.$$

A review of different primal-dual interior point path-following methods in Alizadeh et al. (1998) showed that algorithms using the upper triangular part of of this symmetric version were the most stable in computations. They also proved that the Jacobian matrix of the corresponding well-constrained KKT equality conditions being full rank was equivalent to complementary slackness and nondegeneracy of the optimal solution to the SDP. Thus, we will follow this approach and their notation to yield a well-constrained polynomial

system encoding the KKT conditions. For succinctness, let $c = k + n + n^2$ and $\boldsymbol{v}(\boldsymbol{\delta})$ be the vector of length c corresponding to the variables of $\mathbf{F}$, namely

$$\boldsymbol{v}(\boldsymbol{\delta}) = \begin{pmatrix} \text{svec}(X(\boldsymbol{\delta})) \\ y(\boldsymbol{\delta}) \\ \text{svec}(S(\boldsymbol{\delta})) \end{pmatrix},$$

where the operator svec is defined as

$$\text{svec}(M) = (m_{11}, \sqrt{2}m_{12}, \ldots, \sqrt{2}m_{1n}, m_{22}, \ldots, \sqrt{2}m_{2n}, \ldots, m_{nn})^T.$$

We collect all solutions to the equality conditions of the KKT system in the set

$$\mathcal{V}(\boldsymbol{\delta}) = \{\boldsymbol{v} \in \mathbb{C}^c \mid \boldsymbol{F}(\boldsymbol{v}; \boldsymbol{\delta}) = 0\}.$$

Hence, optimal solutions are those in $\mathcal{V}(\boldsymbol{\delta}) \cap \mathbb{R}^c$ which satisfy the inequalities in (3). Moreover, convexity shows that if there are finitely many points in $\mathcal{V}(\boldsymbol{\delta})$, only one of them can be in $\mathcal{V}(\boldsymbol{\delta}) \cap \mathbb{R}^c$ and satisfy the inequalities in (3), which will be denoted by $\hat{\boldsymbol{v}}(\boldsymbol{\delta})$. By Assumption 3, $\hat{\boldsymbol{v}}(\boldsymbol{\delta})$ is well-defined in a neighborhood of 0.

Writing $\mathcal{A}(\boldsymbol{\delta}) = \big(\text{svec}(A_1 + \sum_{j=1}^{\ell} \delta_j E_{j1}), \ldots, \text{svec}(A_k + \sum_{j=1}^{\ell} \delta_j E_{jk})\big)^T$, the equality conditions (4) can be reformulated as

$$\boldsymbol{F}(\boldsymbol{v}; \boldsymbol{\delta}) = \begin{pmatrix} \mathcal{A}(\boldsymbol{\delta})\text{svec}(X) - (b + G\boldsymbol{\delta}) \\ \text{svec}(C + \sum_{j=1}^{\ell} \delta_j D_j) - \mathcal{A}(\boldsymbol{\delta})^T y - \text{svec}(S) \\ \text{svec}(SX + XS)/2 \end{pmatrix} = 0 \tag{5}$$

and its Jacobian matrix with respect to the variables $\boldsymbol{v}$ is

$$J_{\boldsymbol{v}}\boldsymbol{F}(\boldsymbol{v}; \boldsymbol{\delta}) = \begin{pmatrix} \mathcal{A}(\boldsymbol{\delta}) & 0 & 0 \\ 0 & \mathcal{A}(\boldsymbol{\delta})^T & I_{\frac{n+n^2}{2}} \\ S \otimes_s I_n & 0 & X \otimes_s I_n \end{pmatrix}. \tag{6}$$

For any two square matrices K_1 and K_2 and a symmetric matrix J, the *symmetric Kronecker product*, denoted by $\otimes_s$, can be defined as a mapping on a vector $\text{svec}(J)$:

$$(K_1 \otimes_s K_2)\text{svec}(J) := \frac{1}{2}\text{svec}\big(K_2 J K_1^T + K_1 J K_2^T\big),$$

see de Klerk (2006); Todd et al. (1998) for more details. Let

$$\begin{aligned} \mathcal{D} &= (\text{svec}(D_1), \ldots, \text{svec}(D_\ell)), \\ \mathcal{E} &= (\text{svec}(E_{11}), \ldots, \text{svec}(E_{1k}), \text{svec}(E_{21}), \ldots, \text{svec}(E_{2k}), \ldots, \text{svec}(E_{\ell k})), \end{aligned}$$

and $\bar{\mathcal{E}}$ be the $k \times \ell$ matrix whose $(i,j)^{\text{th}}$ entry is $\text{svec}(E_{ji})^T\text{svec}(X)$. The partial derivative of $\boldsymbol{F}$ with respect to $\boldsymbol{\delta}$ is

$$\frac{\partial \boldsymbol{F}}{\partial \boldsymbol{\delta}} = \begin{pmatrix} \bar{\mathcal{E}} - G \\ \mathcal{D} - \mathcal{E}(I_\ell \otimes y) \\ \mathbf{0} \end{pmatrix}. \tag{7}$$

By Assumption 3 and the implicit function theorem, $J_{\boldsymbol{v}}\boldsymbol{F}(\hat{\boldsymbol{v}}(0); 0)$ is nonsingular so that $J_{\boldsymbol{v}}\boldsymbol{F}(\hat{\boldsymbol{v}}(\boldsymbol{\delta}); \boldsymbol{\delta})$ is nonsingular for $\boldsymbol{\delta}$ in a neighborhood of 0. In particular, by (Haeberly, 1998, Theorem 3.1), one can replace the analytic condition in Def. 2 with $J_{\boldsymbol{v}}\boldsymbol{F}(\hat{\boldsymbol{v}}(\boldsymbol{\delta}); \boldsymbol{\delta})$ being nonsingular so that the implicit function theorem provides the analyticity of $\hat{\boldsymbol{v}}(\boldsymbol{\delta})$.

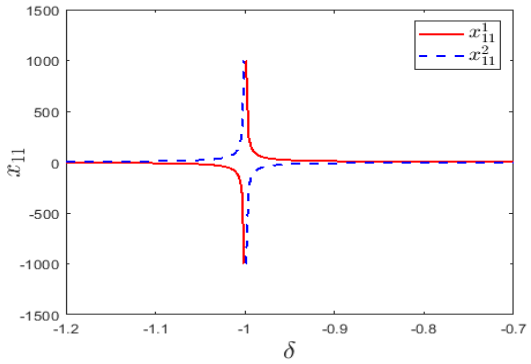

Figure 1: The x_{11} entry of the two solution paths of $\boldsymbol{F} = 0$.

Example 3.1. *For the compact set $B = [-2, 1] \subset \mathbb{R}$, we aim to find the MAPS of B containing the origin for the following:*

$$C = I_2, \quad D_1 = \mathbf{0}, \quad A_1 = \begin{pmatrix} 0 & 1 \\ 1 & 0 \end{pmatrix}, \quad E_{11} = \begin{pmatrix} 0 & 1 \\ 1 & 0 \end{pmatrix}, \quad G = 0, \quad \textit{and} \quad b_1 = 2$$

so that (1) and (2) yield

$$\begin{array}{lll} \textit{minimize} & x_{11} + x_{22} & \qquad \textit{maximize} \quad 2(1+\delta)y \\ \textit{s.t.} & 2(1+\delta)x_{12} = 2 & \qquad \textit{s.t.} \\ & X = \begin{bmatrix} x_{11} & x_{12} \\ x_{12} & x_{22} \end{bmatrix} \succeq 0 & \qquad S = \begin{bmatrix} 1 & y \\ -(1+\delta)y & 1 \end{bmatrix} \succeq 0. \end{array} \tag{8}$$

The corresponding KKT equality conditions are:

$$\boldsymbol{F} = \begin{pmatrix} \sqrt{2}(1+\delta)x_{12} - \sqrt{2} \\ s_{11} - 1 \\ \sqrt{2}s_{12} + \sqrt{2}(1+\delta)y \\ s_{11}x_{11} + s_{12}x_{12} \\ \frac{1}{\sqrt{2}}(s_{11}x_{12} + s_{12}x_{22} + x_{11}s_{12} + x_{12}s_{22}) \\ s_{12}x_{12} + s_{22}x_{22} \end{pmatrix} = 0. \tag{9}$$

There are two sets of parameterized solutions, namely

$$\boldsymbol{v}^i(\delta) = (x_{11}^i(\delta), x_{12}^i(\delta), x_{22}^i(\delta), y^i(\delta), s_{11}^i(\delta), s_{12}^i(\delta), s_{22}^i(\delta))$$

for $i = 1, 2$ with

$$\boldsymbol{v}^1(\delta) = \left(\tfrac{1}{1+\delta}, \tfrac{1}{1+\delta}, \tfrac{1}{1+\delta}, \tfrac{1}{1+\delta}, 1, -1, 1\right) \quad \textit{and} \quad \boldsymbol{v}^2(\delta) = \left(-\tfrac{1}{1+\delta}, \tfrac{1}{1+\delta}, -\tfrac{1}{1+\delta}, -\tfrac{1}{1+\delta}, 1, 1, 1\right).$$

Figure 3.1 plots the x_{11} entry with respect to δ for the two solutions of $\boldsymbol{F} = 0$. Since $x_{11} \geq 0$ is a necessary condition for $X \succeq 0$, it is easy to verify that

$$\hat{\boldsymbol{v}}(\delta) = \begin{cases} \boldsymbol{v}^1(\delta) & \textit{if } \delta > -1, \\ \boldsymbol{v}^2(\delta) & \textit{if } \delta < -1. \end{cases}$$

In particular, Figure 3.1 clearly shows that the optimal solution path $\hat{\boldsymbol{v}}(\delta)$ is not analytic at $\delta = -1$. Relating to the invertibility of the Jacobian, this also matches since

$$\det J_{\boldsymbol{v}}\boldsymbol{F}(\boldsymbol{v}^1(\delta); \delta) = 4(1+\delta) = -\det J_{\boldsymbol{v}}\boldsymbol{F}(\boldsymbol{v}^2(\delta); \delta)$$

vanishes at $\delta = -1$. Thus, the MAPS with respect to $B = [-2, 1]$ is $U = (-1, 1]$ which is open relative to B with boundary $\partial U = \{-1, 1\}$.

We first establish an important result regarding limiting behavior of nonsingularity of the Jacobian matrix and feasibility. It is well known that the limiting point of feasible points need not be feasible. However, with the extra condition of the nonsingularity of the Jacobian matrix at these feasible points, the limiting point must be feasible.

Lemma 1. *Let $\boldsymbol{\delta} : [0,1] \to U$ be a semialgebraic path with $\boldsymbol{v}(\boldsymbol{\delta}(t)) = \hat{\boldsymbol{v}}(\boldsymbol{\delta}(t))$ for $t \in [0,1)$. If $J_{\boldsymbol{v}}\boldsymbol{F}(\hat{\boldsymbol{v}}(\boldsymbol{\delta}(t)); \boldsymbol{\delta}(t))$ is nonsingular for $t \in [0,1]$, then $\lim_{t\to 1^-} v(\boldsymbol{\delta}(t)) = \hat{\boldsymbol{v}}(\boldsymbol{\delta}(1))$.*

Proof. Let $X(\boldsymbol{\delta}(t))$ and $S(\boldsymbol{\delta}(t))$ be the corresponding matrices described by $v(\boldsymbol{\delta}(t))$. Note that the nondegeneracy and complimentary slackness of the optimal solution are equivalent to the Jacobian matrix (6) being full rank. Along with lower semicontinuity of matrix ranks, this shows that, for $t \in [0,1)$,

$$\operatorname{rank} X(\boldsymbol{\delta}(t)) + \operatorname{rank} S(\boldsymbol{\delta}(t)) = n$$

and thus both $\operatorname{rank} X(\boldsymbol{\delta}(t))$ and $\operatorname{rank} S(\boldsymbol{\delta}(t))$ are constant on $t \in [0,1)$. Since all of the nonzero eigenvalues of $X(\boldsymbol{\delta}(t))$ and $S(\boldsymbol{\delta}(t))$ are positive at $t = 0$, they must remain positive for all $t \in [0,1)$ showing that (3) holds for $t \in [0,1)$. Thus, the inequalities must hold in the limit as t approaches 1. Hence, $v(\boldsymbol{\delta}(1))$ is also feasible and since $J_{\boldsymbol{v}}\boldsymbol{F}(\hat{\boldsymbol{v}}(\boldsymbol{\delta}(t)); \boldsymbol{\delta}(t))$ is nonsingular, $\boldsymbol{v}(\boldsymbol{\delta}(1)) = \hat{\boldsymbol{v}}(\boldsymbol{\delta}(1))$ is the unique optimal solution.

The following describes the boundary ∂U of the maximal analytic perturbation set U.

Proposition 1. *If $\boldsymbol{\delta}^* \in \partial U$, then one of the following must hold:*

(a) $\boldsymbol{\delta}^* \in \partial B$,

(b) $\lim_{\boldsymbol{\delta}\in U\to\boldsymbol{\delta}^*} \hat{\boldsymbol{v}}(\boldsymbol{\delta})$ *diverges, or*

(c) $\lim_{\boldsymbol{\delta}\in U\to\boldsymbol{\delta}^*} \hat{\boldsymbol{v}}(\boldsymbol{\delta})$ *exists, say $\hat{\boldsymbol{v}}(\boldsymbol{\delta}^*)$, such that $J_{\boldsymbol{v}}\boldsymbol{F}(\hat{\boldsymbol{v}}(\boldsymbol{\delta}^*); \boldsymbol{\delta}^*)$ is singular.*

Proof. If $\boldsymbol{\delta}^* \notin \partial B$ and $\hat{\boldsymbol{v}}(\boldsymbol{\delta}^*)$ exists, then it immediately follows from the implicit function theorem that $J_{\boldsymbol{v}}\boldsymbol{F}(\hat{\boldsymbol{v}}(\boldsymbol{\delta}^*); \boldsymbol{\delta}^*)$ must be singular.

In particular, these conditions yield that the boundary is semialgebraic.

Corollary 1. *The boundary of U is a semialgebraic set.*

Proof. Since the boundary of B is a semialgebraic set by Assumption 1, the three items in Proposition 1 describing ∂U are clearly semialgebraic conditions.

The following shows that MAPS are open relative to the compact bounding set B.

Theorem 2. *The maximal analytic perturbation set $U \subset B$ is open relative to B.*

Proof. Fix $\boldsymbol{\delta}^* \in U$. Since U is a connected set containing 0 in the interior and the boundary of U is a semialgebraic set, we know that the interior of U is path connected. Hence, let $\boldsymbol{\delta} : [0,1] \mapsto U$ be a smooth path such that $\boldsymbol{\delta}(0) = 0$, $\boldsymbol{\delta}(1) = \boldsymbol{\delta}^*$, and $\boldsymbol{\delta}(t)$ is in the interior of U for $t \in [0,1)$. Since $J_{\boldsymbol{v}}\boldsymbol{F}(\hat{\boldsymbol{v}}(\boldsymbol{\delta}(0)); \boldsymbol{\delta}(0))$ is invertible, the implicit function theorem yields that there exists a function $\boldsymbol{v}(\boldsymbol{\delta}(t))$ which is analytic for $t \in [0, \epsilon)$ for some $\epsilon > 0$ such that $\boldsymbol{v}(\boldsymbol{\delta}(0)) = \hat{\boldsymbol{v}}(\boldsymbol{\delta}(0))$, i.e., the optimal solution at 0, such that

$\boldsymbol{F}(\boldsymbol{v}(\boldsymbol{\delta}(t)); \boldsymbol{\delta}(t)) = 0$ and $J_{\boldsymbol{v}}\boldsymbol{F}(\boldsymbol{v}(\boldsymbol{\delta}(t)); \boldsymbol{\delta}(t))$ is full rank for all $t \in [0, \epsilon)$. Since $\boldsymbol{\delta}(t)$ lies in the interior of U for $t \in [0, 1)$, one immediately has $\epsilon \geq 1$ so that by Lemma 1, $\boldsymbol{v}(\boldsymbol{\delta}(1)) = \lim_{t \to 1^-} \boldsymbol{v}(\boldsymbol{\delta}(t))$ is well-defined.

Hence, repeating a similar argument as above, the implicit function theorem shows that there is an open neighborhood of $\boldsymbol{\delta}^*$, say $U_{\boldsymbol{\delta}^*}$, such that $\boldsymbol{\delta}^* \in U_{\boldsymbol{\delta}^*} \cap B \subset U \cap B$. Therefore, U is open in B.

Remark 1. The MAPS U differs from the maximum set where a robust solution exists, e.g., see Ben-Tal et al. (1998); EL Ghaoui et al. (1998), as this does not consider the feasibility of $\hat{\boldsymbol{v}}(0)$ for perturbations $\delta \in U$. Rather, the MAPS exams when there is no longer any feasible solutions connecting smoothly. Moreover, Hauenstein et al. (2022) explores the nonlinearity interval studied which is the MAPS restricted to a single parameter.

With these characterizations of U and ∂U, the aim is to simultaneously compute $\hat{\boldsymbol{v}}(\delta)$ on U and identify the boundary ∂U. Our approach for this computation is to utilize derivative information of the solution and recover the solution along different perturbation directions. In particular, the following uses the Davidenko differential equation to convert the problem of solving a system of polynomials with changing coefficients to solve a system of first-order quasilinear partial differential equations (PDEs) with the perturbation parameters as variables.

The Davidenko equation from Kalaba et al. (1977) together with the implicit function theorem provides that the total derivative of the i^{th} equation in (5) with respect to δ_j is

$$d_{\delta_j}\boldsymbol{F}_i = \frac{\partial \boldsymbol{F}_i}{\partial \boldsymbol{v}} \frac{d\boldsymbol{v}}{d\delta_j} + \frac{\partial \boldsymbol{F}_i}{\partial \delta_j} = 0.$$

This equation governs how the solution of (5) travels along any scalar perturbation variable. Assembling all these differential equations with index (i, j) yields the system

$$D\boldsymbol{F} = J_{\boldsymbol{v}}\boldsymbol{F}\frac{\partial \boldsymbol{v}}{\partial \boldsymbol{\delta}} + \frac{\partial \boldsymbol{F}}{\partial \boldsymbol{\delta}} = \boldsymbol{0} \tag{10}$$

Since $J_{\boldsymbol{v}}\boldsymbol{F}$ is invertible in U, multiplying by $(J_{\boldsymbol{v}}\boldsymbol{F})^{-1}$ on the left yields

$$\frac{\partial \boldsymbol{v}}{\partial \boldsymbol{\delta}} = -(J_{\boldsymbol{v}}\boldsymbol{F})^{-1}\frac{\partial \boldsymbol{F}}{\partial \boldsymbol{\delta}}. \tag{11}$$

Since the highest order derivatives, namely $\frac{\partial \boldsymbol{v}}{\partial \boldsymbol{\delta}}$, appear linearly while $\boldsymbol{v}(\boldsymbol{\delta})$ appears nonlinearly on the right-hand side, namely $-(J_{\boldsymbol{v}}\boldsymbol{F})^{-1}\frac{\partial \boldsymbol{F}}{\partial \boldsymbol{\delta}}$, (11) is a system of quasilinear PDEs. Although not linear, quasilinearity still provides a wealth of results, e.g., see Evans (2010). In particular, the solving scheme described in Section 5 considers solving along directions $\boldsymbol{\alpha}$ emanating from the origin. Thus, one can multiply both sides of (11) by $\boldsymbol{\alpha}$ to yield

$$\frac{\partial \boldsymbol{v}}{\partial \boldsymbol{\delta}}\boldsymbol{\alpha} = -(J_{\boldsymbol{v}}\boldsymbol{F})^{-1}\frac{\partial \boldsymbol{F}}{\partial \boldsymbol{\delta}}\boldsymbol{\alpha}. \tag{12}$$

To properly define the domain and boundary for this PDE system, let $\underline{U} = U \setminus \partial U$ be the maximum proper open subset of U. Then, by (Moerdijk and Reyes, 1991, Lemma 1.4), there exists a smooth characteristic function K whose support is $\underline{U}$. Since K does not vanish on $\underline{U}$, K has the same sign at all points of $\underline{U}$. By replacing K by $-K$ if necessary, we can assume without loss of generality that $K > 0$ on $\underline{U}$. With this, we can define a family of subsets $\{W_\epsilon\}_{\epsilon > 0}$ contained in U as follows:

$$W_\epsilon = \{\boldsymbol{\delta} \in U \mid K(\boldsymbol{\delta}) > \epsilon\}.$$

Lemma 3. *There exists $\eta > 0$ such that, for all $\epsilon \in (0, \eta)$, the boundary, ∂W_ϵ, of W_ϵ is smooth and $W_\epsilon \to \underline{U}$ as $\epsilon \to 0^+$ in Hausdorff distance.*

PROOF. By Sard's theorem, e.g., see Sard (1942), there exists $\eta > 0$ such that, for all $\epsilon \in (0, \eta)$, $K(\delta) = \epsilon$ defines a smooth curve. By definition of K, the closure of W_ϵ, namely $\bar{W}_\epsilon$, is a proper closed subset of U with smooth boundary. The Hausdorff distance between the set W_ϵ and U is defined as

$$d_K(U, W_\epsilon) = \max\left\{\sup_{\boldsymbol{\delta}\in U} d(\boldsymbol{\delta}, W_\epsilon), \sup_{\boldsymbol{\delta}'\in W_\epsilon} d(\boldsymbol{\delta}', U)\right\},$$

where the distance between a point x and a set Y is defined as

$$d(x, Y) = \inf_{y\in Y} d(x, y)$$

with $d(x, y) = ||x - y||$ being the Euclidean distance. Since $\underline{U} = \cup_{\alpha>0} K^{-1}(\alpha) \cap U$ and, for $\epsilon > 0$, $W_\epsilon \subset \underline{U}$ with $W_\epsilon = \cup_{\alpha>\epsilon} K^{-1}(\epsilon) \cap U$, one clearly has $\lim_{\epsilon\to 0^+} d_K(\underline{U}, W_\epsilon) = 0$ since K is a C^∞ function.

It immediate follows from Lemma 3 and Theorem 2 that the function $G_\epsilon = \hat{\boldsymbol{v}}|_{\partial W_\epsilon}$ obtained by restricting $\hat{\boldsymbol{v}}(\boldsymbol{\delta})$ to ∂W_ϵ is analytic as summarized in the following.

Corollary 2. *There exists $\eta > 0$ such that for all $\epsilon \in (0, \eta)$, G_ϵ is analytic on ∂W_ϵ.*

4. Well-posedness of the governing PDE

With a smooth boundary condition, the following shows that the optimal solution is the unique solution to the system of quasilinear PDEs. Although Corollary 1 shows that the boundary is semialgebraic, the current aim is not to directly compute a closed form description of the boundary. Instead, the current aim here is the well-posedness of the governing PDEs to provide theoretical support for numerically approximating the maximum analytic perturbation set in Section 5, which presents a numerical algorithm to solve such a system of PDEs with *a priori* unknown boundary.

Theorem 4. *The following is well-posed and its unique solution is the optimal solution $\hat{\boldsymbol{v}}$ on $\bar{W}_\epsilon$:*

$$\begin{cases} \dfrac{\partial \boldsymbol{v}}{\partial \boldsymbol{\delta}} &= -(J_{\boldsymbol{v}}\boldsymbol{F})^{-1}\frac{\partial \boldsymbol{F}}{\partial \boldsymbol{\delta}} \qquad \text{in } W_\epsilon, \\ \boldsymbol{v}(\boldsymbol{0}) &= \boldsymbol{v}_0. \end{cases} \tag{13}$$

PROOF. First, it is clear from the derivation of system (13) that the optimal solution $\hat{\boldsymbol{v}}$ is a solution. So, it suffices to prove that it is unique. To that end, assume $\boldsymbol{u}$ also solves (13). Then, $\boldsymbol{w} = \hat{\boldsymbol{v}} - \boldsymbol{u}$ satisfies $\dfrac{\partial \boldsymbol{w}}{\partial \boldsymbol{\delta}} = 0$ on W_ϵ and $\boldsymbol{w}(\boldsymbol{0}) = 0$. Integration and the initial condition imply $\boldsymbol{w} = \boldsymbol{0}$ on $\bar{W}_\epsilon$. Thus, the optimal solution is the unique solution to the system (13) on $\bar{W}_\epsilon$.

Note that system (13) is not a "typical" PDE system as the initial condition is defined at a point rather than the boundary of the domain of the governing system. However, with knowledge of the derivative in all directions at any given point in W_ϵ, methods

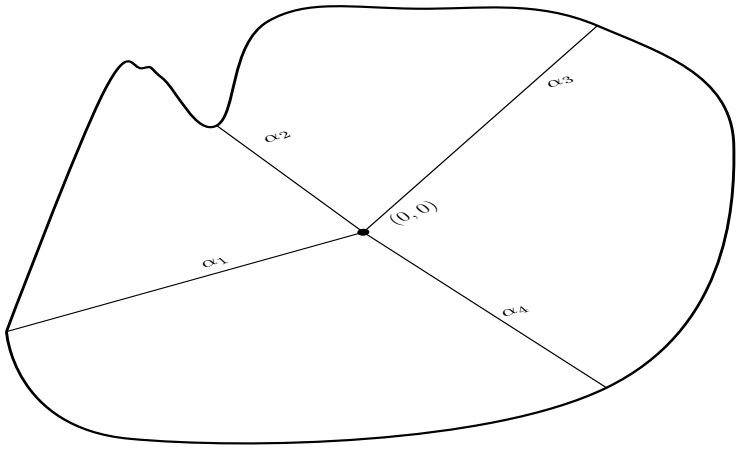

Figure 2: Illustration of approximating the boundary of W_ϵ along different choices of characteristics.

can be employed to systematically solve this system. One crude approach would be to establish a mesh on B and solving at each of the mesh points starting at the origin. The approach in Section 5 is to utilize polar coordinates and sweep through the parameter space along different choices of characteristics via (12) as illustrated in Figure 2.

In order to make Theorem 4 effective, we need a concrete criteria to determine whether a point along the characteristic curve is within the set or not. By Assumption 3 and Theorem 2, we have the following property of the solution to (1) and (2) which will be used in Section 5.3 to numerically identify the boundary.

Proposition 2. *The minimum eigenvalues, $\lambda_{ms}(\delta)$ and $\lambda_{mx}(\delta)$, of matrices $S(\delta)$ and $X(\delta)$, respectively, are identically zero in U. In addition, along any direction α, the derivative of $\lambda_{ms}(\delta)$ and $\lambda_{mx}(\delta)$ along any characteristic curve with respect to its parameter is zero in $\overline{W}_\epsilon$.*

Proof. This trivially follows from the complimentary slackness condition $XS = 0$.

5. Sweeping Euler scheme

Building on the theoretical foundation, the following develops a second-order numerical scheme, namely a Sweeping Euler Scheme (SES), to solve the parametric SDPs (1) and (2). This scheme consists of three components: discretization of the parameter space, local solver, and a boundary threshold criterion.

5.1. Discretization

The first component is to discretize the parameter space. We first reparameterize the parameter space using spherical coordinates with the following representation:

$$\boldsymbol{\delta}(\theta_1, \theta_2, \ldots, \theta_{\ell-1}) = s\boldsymbol{\alpha} = s \begin{pmatrix} \cos(\theta_1) \\ \sin(\theta_1)\cos(\theta_2) \\ \sin(\theta_1)\sin(\theta_2)\cos(\theta_3) \\ \vdots \\ \sin(\theta_1)\cdots\sin(\theta_{\ell-2})\cos(\theta_{\ell-1}) \\ \sin(\theta_1)\cdots\sin(\theta_{\ell-2})\sin(\theta_{\ell-1}) \end{pmatrix}.$$

For $\theta_1, \ldots, \theta_{\ell-2} \in [0, \pi)$ and $\theta_{\ell-1} \in [0, 2\pi)$, the direction vector $\boldsymbol{\alpha}$ sweeps the entire $(\ell-1)$-dimensional unit sphere. Let R be the radius of an sphere centered at the origin in $\mathbb{R}^\ell$ which contains B. Thus, we discretize both in the directions with step size $\Delta\theta_i$ and the length on $[0, R]$ using step size Δs.

5.2. Local solver

The second component is solving (12) iteratively along each direction selected by the directional sweeping component. In our computations, we apply Heun's method to (12) along the characteristic determined by the direction $\boldsymbol{\alpha}$ starting at the origin. Here, we abuse the notation of the directional vector $\boldsymbol{\alpha}$ to denote $\boldsymbol{\alpha}(k_1\Delta\theta_1, k_2\Delta\theta_2, \ldots, k_{\ell-1}\Delta\theta_{\ell-1})$. Then, the i^{th} mesh point along a given direction $\boldsymbol{\alpha}$ is represented by $s_i = i\Delta s$. Let $\boldsymbol{\delta_i} = s_i\boldsymbol{\alpha}$ and suppose that V_i to represent the approximation of $\boldsymbol{v}(\boldsymbol{\delta})$ at $\boldsymbol{\delta}_i$ along $\boldsymbol{\alpha}$. In addition, we use $H_i(V_j)$ to represent the approximation of $-(J_{\boldsymbol{v}}\boldsymbol{F})^{-1}\frac{\partial \boldsymbol{F}}{\partial \boldsymbol{\delta}}\boldsymbol{\alpha}$ at $\boldsymbol{\delta}_i$ and V_j. The numerical scheme solving (12) starting at 0 is

$$\begin{aligned} V_0 &= \boldsymbol{v}_0 \\ \tilde{V}_{i+1} &= V_i + \Delta s H_i(V_i) \\ V_{i+1} &= V_i + \frac{\Delta s}{2}\Big(H_i(V_i) + H_{i+1}(\tilde{V}_{i+1})\Big) \quad \text{for } i \geq 0. \end{aligned} \tag{14}$$

Although this numerical scheme is known to have global order two, e.g., see Ackleh et al. (2009), to the best of our knowledge, an explicit upper bound on the global error of this method for a system of ODEs has not been provided. We provide such a bound in the following with $E_i = \|\boldsymbol{v}(\boldsymbol{\delta}_i) - V_i\|$ denoting the global error at $s = s_i$ while err_i denotes the local error at s_i. In the following, we let $h = \Delta s$, $\boldsymbol{v}(s) = \boldsymbol{v}(\boldsymbol{\delta}(s))$, and $H(s, \boldsymbol{v}(s)) = -(J_{\boldsymbol{v}}\boldsymbol{F})^{-1}\frac{\partial F}{\partial \boldsymbol{\delta}}\boldsymbol{\alpha}\Big|_{\left(\boldsymbol{\delta}(s), \boldsymbol{v}(\boldsymbol{\delta}(s))\right)}$ for simplicity.

Theorem 5. *For* (14)*, there exist constants* M *and* D*, defined in* (16) *and* (20)*, respectively, which are independent of step size* h *such that the local error satisfies*

$$err_i \leq Dh^3,$$

and the global error satisfies

$$E_i \leq \frac{D}{M}(e^{Ms_i} - 1)h^2.$$

Proof. Consider the function $\Phi : \mathbb{R} \times \mathbb{R}^c \times \mathbb{R} \to \mathbb{R}^c$ defined by

$$\Phi(s, \boldsymbol{v}(s), h) = H(s, \boldsymbol{v}(s)) + H(s + h, hH(s, \boldsymbol{v}(s)) + \boldsymbol{v}(s)).$$

On the MAPS U, $H(s, \boldsymbol{v}(s))$ is analytic, thus Lipschitz continuous in s and $\boldsymbol{v}$, so we can obtain that

$$\|\Phi(s, \boldsymbol{v}_1, h) - \Phi(s, \boldsymbol{v}_2, h)\| \leq M\|\boldsymbol{v}_1 - \boldsymbol{v}_2\|, \tag{15}$$

where

$$M = \max_{t\in[0,1]}\Big(\left\|\frac{\partial H}{\partial \boldsymbol{v}}(s, t\boldsymbol{v}_1 + (1-t)\boldsymbol{v}_2)\right\|, \left\|\frac{\partial H}{\partial \boldsymbol{v}}(s + h, t\boldsymbol{v}_1 + (1-t)\boldsymbol{v}_2)\right\|\Big). \tag{16}$$

Next, we consider the function

$$d(s, \boldsymbol{v}(s), h) = \boldsymbol{v}(s + h) - \boldsymbol{v}(s) - \frac{h}{2}\Phi(s, \boldsymbol{v}(s), h).$$

For $j = 1, \ldots, c$, let $\boldsymbol{v}^j$ and H^j denote the j^{th} element in the corresponding vector. By Taylor expansion,

$$\boldsymbol{v}^j(s+h) = \boldsymbol{v}^j(s) + h\frac{d\boldsymbol{v}^j}{ds}(s) + \frac{h^2}{2}\frac{d^2\boldsymbol{v}^j}{ds^2}(s) + \frac{h^3}{3!}\frac{d^3\boldsymbol{v}^j}{ds^3}(s) + \frac{h^4}{4!}\frac{d^4\boldsymbol{v}^j}{ds^4}(\eta_1) \tag{17}$$

and

$$\begin{aligned} H^j\big(s+h, \boldsymbol{v}(s) + hH(s,\boldsymbol{v}(s))\big) &= H^j(s,\boldsymbol{v}(s)) \\ &+ h\frac{\partial H^j}{\partial s}(s,\boldsymbol{v}(s)) + \frac{\partial H^j}{\partial \boldsymbol{v}}(s,\boldsymbol{v}(s))hH(s,\boldsymbol{v}(s)) \\ &+ \frac{h^2}{2}\frac{\partial^2 H^j}{\partial s^2}(s,\boldsymbol{v}(s)) + 2\frac{h}{2}\frac{\partial^2 H^j}{\partial s\partial \boldsymbol{v}}hH(s,\boldsymbol{v}(s)) \\ &+ \frac{1}{2}\big(hH(s,\boldsymbol{v}(s))\big)^T\frac{\partial^2 H^j}{\partial \boldsymbol{v}^2}(s,\boldsymbol{v}(s))hH(s,\boldsymbol{v}(s)) \\ &+ \frac{h^3}{3!}\frac{\partial^3 H^j}{\partial s^3}(\eta_2,\boldsymbol{v}(s)) + 3\frac{h^2}{3!}\frac{\partial^3 H^j}{\partial s^2\partial \boldsymbol{v}}(\eta_3,\xi_1)hH(s,\boldsymbol{v}(s)) \\ &+ 3\frac{h}{3!}\big(hH(s,\boldsymbol{v}(s))\big)^T\frac{\partial^3 H^j}{\partial s\partial \boldsymbol{v}^2}(\eta_4,\xi_2)hH(s,\boldsymbol{v}(s)) \\ &+ \frac{1}{3!}\frac{\partial^3 H^j}{\partial \boldsymbol{v}^3}(s,\xi_3)\otimes\big(hH(s,\boldsymbol{v}(s))\big), \end{aligned} \tag{18}$$

where $\eta_k \in [s, s+h]$ for $k = 1, \ldots, 4$ and ξ_q for $q \in 1, 2, 3$ is a point on the line segment connecting $\boldsymbol{v}(s)$ and $\boldsymbol{v}(s) + hH(s,\boldsymbol{v}(s))$. The matrix $\frac{\partial^2 H^j}{\partial \boldsymbol{v}^2}$ and tensor $\frac{\partial^3 H^j}{\partial \boldsymbol{v}^3}$ are the second and third derivative of H^j with respect to V, respectively. In particular, if A is a $p\times p\times p$ tensor and $b \in \mathbb{R}^p$, then

$$A \otimes b = \sum_{i,j,k}^{p} a_{ijk}b_ib_jb_k$$

From (12), we have that

$$\begin{aligned} \frac{d\boldsymbol{v}^j}{ds}(s) &= H^j(s,\boldsymbol{v}(s)) \\ \frac{d^2\boldsymbol{v}^j}{ds^2}(s) &= \frac{dH^j}{ds}(s,\boldsymbol{v}(s)) = \frac{\partial H^j}{\partial s}(s,\boldsymbol{v}(s)) + \frac{\partial H^j}{\partial \boldsymbol{v}}(s,\boldsymbol{v}(s))H(s,\boldsymbol{v}(s)) \\ \frac{d^3\boldsymbol{v}^j}{ds^3}(s) &= \frac{\partial^2 H^j}{\partial s^2}(s,\boldsymbol{v}(s)) + 2\frac{\partial^2 H^j}{\partial s\partial \boldsymbol{v}}(s,\boldsymbol{v}(s))H(s,\boldsymbol{v}(s)) \\ &+ \frac{\partial H^j}{\partial \boldsymbol{v}}(s,\boldsymbol{v}(s))\frac{\partial H}{\partial \boldsymbol{v}}(s,\boldsymbol{v}(s))H(s,\boldsymbol{v}(s)) \\ &+ \frac{\partial H^j}{\partial \boldsymbol{v}}(s,\boldsymbol{v}(s))\frac{\partial H}{\partial s}(s,\boldsymbol{v}(s)) + \big(H(s,\boldsymbol{v}(s))\big)^T\frac{\partial^2 H^j}{\partial \boldsymbol{v}^2}(s,\boldsymbol{v}(s))H(s,\boldsymbol{v}(s)). \end{aligned} \tag{19}$$

Using (17)-(19), we have

$$\begin{aligned} d^j(s,\boldsymbol{v}(s),h) &= \frac{h^3}{6}\frac{\partial H^j}{\partial \boldsymbol{v}}(s,\boldsymbol{v}(s))\frac{\partial H}{\partial \boldsymbol{v}}(s,\boldsymbol{v}(s))H(s,\boldsymbol{v}(s)) + \frac{h^3}{6}\frac{\partial H^j}{\partial \boldsymbol{v}}(s,\boldsymbol{v}(s))\frac{\partial H}{\partial s}(s,\boldsymbol{v}(s)) \\ &- \frac{h^3}{12}\frac{\partial^2 H^j}{\partial s^2}(s,\boldsymbol{v}(s)) - \frac{h^3}{6}\frac{\partial^2 H^j}{\partial s\partial \boldsymbol{v}}(s,\boldsymbol{v}(s))H(s,\boldsymbol{v}(s)) \\ &- \frac{h^3}{12}\big(H(s,\boldsymbol{v}(s))\big)^T\frac{\partial^2 H^j}{\partial \boldsymbol{v}^2}H(s,\boldsymbol{v}(s)) + \frac{h^4}{4!}\frac{d^4V}{ds^4}(s) - R \end{aligned}$$

where R represents the last four terms in (18). Define

$$\begin{aligned} L &= \max_{1\le j\le c}\ \max_{s\in[0,s_{\alpha,\delta_0}]} |\boldsymbol{v}^j(s)|, \\ L_1 &= \max_{1\le i,j\le c}\ \max_{s\in[0,s_{\alpha,\delta_0}]} \left\{\left|\frac{\partial H^i}{\partial \boldsymbol{v}^j}(s,\boldsymbol{v}(s))\right|, \left|\frac{\partial H^i}{\partial s}(s,\boldsymbol{v}(s))\right|\right\}, \\ L_2 &= \max_{1\le i,j,k\le c}\ \max_{s\in[0,s_{\alpha,\delta_0}]} \left\{\left|\frac{\partial^2 H^i}{\partial \boldsymbol{v}^k\partial \boldsymbol{v}^j}(s,\boldsymbol{v}(s))\right|, \left|\frac{\partial^2 H^i}{\partial s\partial \boldsymbol{v}^j}(s,\boldsymbol{v}(s))\right|, \left|\frac{\partial^2 H^i}{\partial s}(s,\boldsymbol{v}(s))\right|\right\}. \end{aligned}$$

Then, for sufficient small h and $j = 1, \ldots, c$, we have

$$|d^j(s,\boldsymbol{v}(s),h)| \le \frac{h^3}{6}LL_1^2c^2 + \frac{h^3}{6}L_1^2c + \frac{h^3}{12}L_2 + \frac{h^3}{6}LL_2c + \frac{h^3}{12}L^2L_2c^2 + h^3$$

showing that

$$\|d(s, \boldsymbol{v}(s), h)\| \leq Dh^3 \quad \text{where} \quad D = \frac{1}{6}LL_1^2c^2 + \frac{1}{6}L_1^2c + \frac{1}{12}L_2 + \frac{1}{6}LL_2c + \frac{1}{12}L^2L_2c^2 + 1. \tag{20}$$

From the numerical scheme (14), we have

$$V_{i+1} = V_i + \frac{h}{2}\Phi(s_i, V_i, h). \tag{21}$$

By definition of $d(s, \boldsymbol{v}(s), h)$, we obtain

$$V(s_{i+1}) = V(s_i) + \frac{h}{2}\Phi(s_i, V(s_i), h) + d(s_i, V(s_i), j). \tag{22}$$

Subtracting (21) from (22) and applying the triangle inequality yields

$$E_{i+1} \leq E_i + \frac{h}{2}\|\Phi(s_i, V_i, h) - \Phi(s_i, V(s_i), h)\| + \|d(s_i, V(s_i), h)\|.$$

Replacing the last two terms using (15) and (20), we have

$$E_{i+1} \leq E_i \left(1 + \frac{h}{2}M\right) + Dh^3. \tag{23}$$

which implies that

$$E_i \leq \frac{D}{M}(e^{Ms_i} - 1)h^2$$

yielding the global error bound. The local error bound is immediately obtained by assuming there is no error in previous step, i.e., if $E_i = 0$, then $E_{i+1} \leq Dh^3$.

The upshot of Theorem 5 is that our numerical scheme is convergent and consistent, e.g., see Causon and Mingham (2010). One can improve the accuracy and convergence of the local solver by adding an extra correction solving step according to (4) or replace Heun's method with a higher-order Runge–Kutta method. By discretizing over the angles, one can then assemble the solution inside of W_ϵ obtained from the mesh points together using bicubic interpolation method (for two-dimensional perturbations) or nearest-neighbor interpolation (for perturbations in any dimension) to produce numerical solutions to (1) and (2).

5.3. Boundary threshold condition

The third component of the sweeping Euler scheme is to approximate the boundary of MAPS U by checking whether ∂U lies between the current mesh point and the next mesh point for each direction. In addition to checking whether the current mesh point is still within the bounded set B which corresponds to the first criteria in Proposition 1, we need numerical threshold to check for the other two criteria in Proposition 1. Various sweeping approaches have been proposed for algebraic curves to determine if one is near a singular point, e.g., see Hao et al. (2011); Harrington et al. (2020); Piret and Verschelde (2010). The following presents two options resulting from Proposition 2.

Eigenvalue threshold. Inside of U, the minimum eigenvalue of both $X(\boldsymbol{\delta}(s))$ and $S(\boldsymbol{\delta}(s))$ is zero. One option after crossing the boundary is for one of these minimum eigenvalues to become negative. We can use a small negative constant C_1 to decide that a minimum eigenvalue has become negative.

Derivative threshold. From Proposition 2, the derivatives of the minimum eigenvalues, namely $\frac{d\lambda_{ms}}{ds}$ and $\frac{d\lambda_{mx}}{ds}$, are zero inside of U. Hence, we can threshold, say with a positive constant C_2, based on the absolute value of an approximation of these derivatives.

Thresholding on the minimum eigenvalue may be more intuitive since this is the condition to ensure that the matrices remain positive semidefinite. A small negative constant C_1 is chosen instead of 0 due to numerical error. One major disadvantage is the potential difficulty in selecting this constant C_1 since it is challenging to predict the magnitude of deviation of the minimum eigenvalue. This makes the performance of the eigenvalue threshold approach unstable as demonstrated on an example in Table 6.5.

Inside of U, the derivatives of the minimum eigenvalues $\frac{d\lambda_{ms}}{ds}$ and $\frac{d\lambda_{mx}}{ds}$ are both identically zero. At the boundary ∂U, at least one of them becomes undefined due to either divergence to infinity as one approaches the boundary or one of the matrices becomes more rank deficient. This leads us to determine ∂U via one of these derivatives having a sufficiently large magnitude, which can be better detected numerically. Thus, a threshold C_2 is used to check for the derivatives of the eigenvalues which jumps away from zero as they are becoming undefined crossing the boundary. The SES with the eigenvalue as threshold is outlined with the algorithm below.

Algorithm 1 The SES algorithm with eigenvalue threshold

for $i \leftarrow 1 : \ell - 2$ **do** ▷ Discretization
  $\theta_i \leftarrow [0 : \Delta\theta_i : \pi]$
end for
$\theta_{\ell-1} \leftarrow [0 : \Delta\theta : 2\pi]$
$s \leftarrow [0 : \Delta s : R]$
Define $\boldsymbol{\alpha}(\boldsymbol{\theta}) = [\cos(\boldsymbol{\theta}_1), \sin(\boldsymbol{\theta}_1)\cos(\boldsymbol{\theta}_1), \ldots, \sin(\boldsymbol{\theta}_1)\cdots\cos(\boldsymbol{\theta}_{\ell-1}), \sin(\boldsymbol{\theta}_1)\cdots\sin(\boldsymbol{\theta}_{\ell-1})]$
$V(0) = \boldsymbol{v}_0$
for $k_1 \leftarrow 1 : length(\theta_1)$ **do**
  ⋮
  for $k_{\ell-1} \leftarrow 1 : length(\theta_{\ell-1})$ **do**
    for $r \leftarrow 1 : length(s)$ **do** ▷ The local solver
      $V(r+1) \leftarrow V(r) + \Delta s H_r^{k_1,\ldots,k_{\ell-1}}(V(r))\boldsymbol{\alpha}(\theta_1(k_1), \cdots, \theta_{\ell-1}(k_{\ell-1}))$
      $\bar{H} \leftarrow H_r^{k_1,\ldots,k_{\ell-1}}(V(r)) + H_{r+1}^{k_1,\ldots,k_{\ell-1}}(V(r+1))$
      $V(r+1) \leftarrow V(r) + \frac{\Delta s}{2}\bar{H}\boldsymbol{\alpha}(\theta_1(k_1), \cdots, \theta_{\ell-1}(k_{\ell-1}))$
      $Ex, Es \leftarrow \min eig(X(V(r+1))), \min eig(S(V(r+1)))$ ▷ The eigenvalue threshold
      if Ex or $Es < C_1$ **then**
        $b(k_1, \cdots, k_{\ell-1}) = r\boldsymbol{\alpha}(\theta_1(k_1), \cdots, \theta_{\ell-1}(k_{\ell-1}))$ ▷ Record boundary
        $Break$
      end if
    end for
  end for
  ⋮
end for

Example 5.1. *In Example 3.1, the solution as a function of δ on $(-1,\infty)$ is*

$$y=\frac{1}{1+\delta},\quad X=y\begin{pmatrix}1&1\\1&1\end{pmatrix},\quad S=\begin{pmatrix}1&-(1+\delta)y\\-(1+\delta)y&1\end{pmatrix}=\begin{pmatrix}1&-1\\-1&1\end{pmatrix}. \tag{24}$$

One clearly sees that $X\succeq 0$ for $\delta>-1$, X diverges to infinity as $\delta\to-1^+$, and X has a negative eigenvalue when $\delta<-1$. This shows a potential difficulty of observing a negative eigenvalue by having to pass over a divergent point occurring at $\delta=-1$.

On the other hand,

$$\lim_{\delta\to-1^+}-(J_{\boldsymbol{v}}\boldsymbol{F})^{-1}\frac{\partial\boldsymbol{F}}{\partial\delta}=(-\infty,-\infty,-\infty,-\infty,0,0,0)^T$$

which can be used to identify the ill-conditioning of computing the undefined derivative of the minimum eigenvalue of X at the boundary point $\delta=-1$. We return to this example in Section 6.1.

6. Numerical examples

The following applies the sweeping Euler scheme (SES) developed in Section 5 to find the MAPS U for several examples. In particular, Section 6.1 numerically demonstrates second-order convergence and compares the global error bound from Theorem 5 with actual error. Section 6.2 and 6.3 explores two-parameter SDP and three-parameter SDP with known algebraic solutions. Section 6.4 provides a comparison with SDP solvers. Section 6.5 compares two methods of threshold for the SES algorithm and presents an approach to improve the boundary accuracy quickly. All computations were executed using MATLAB running on a 2.5 GHz Intel Core i5-6500 processor.

6.1. Covergence rate and numerical error

For an illustrative demonstration of the convergence rate and numerical error associated with SES, we return to the setup from Exs. 3.1 and 5.1. To numerically demonstrate the second order convergence of SES, we compare the exact optimal value, denoted by $m(\delta)$, at $\delta=0.05$, namely

$$m(0.05)=\frac{2}{1+0.05}=\frac{40}{21}$$

with numerical approximations using various step sizes. The results are summarized in Table 1 which clearly shows second order convergence for this problem.

Table 1: Numerically testing order of convergence.

Step size	Error	Order
1/20	$4.3735\cdot10^{-4}$	
1/40	$1.1260\cdot10^{-4}$	1.9576
1/80	$2.8546\cdot10^{-5}$	1.9798
1/160	$7.1853\cdot10^{-6}$	1.9901
1/320	$1.8024\cdot10^{-6}$	1.9951
1/640	$4.5136\cdot10^{-7}$	1.9976
1/1280	$1.1293\cdot10^{-7}$	1.9988
1/2560	$2.8245\cdot10^{-8}$	1.9994

Next, using a step size of 3/1000, we compare the global error bound from Theorem 5 applied to $m = \frac{2}{1+\delta}$ for $\delta > -1$ with the actual numerical error. Figure 3 shows that the global error bound from Theorem 5 does indeed provide an upper bound on the actual numerical error. As is typical, this error bound can be quite pessimistic, even for this illustrative example, as δ moves towards the boundary of U. Figure 3 provides a clearer picture as to the behavior of the actual numerical error for $\delta < 0$ on the left and $\delta > 0$ on the right with the same step size of 3/1000. As δ becomes more negative, both the upper bound and the actual error increases as shown on the left. As δ becomes more positive, the error is bounded by $2 \cdot 10^{-7}$ as shown on the right. Note that these approximations arise from only knowing the solution at $\delta = 0$. To reduce numerical error, especially as one more towards a point on the boundary of U, one can always use the numerical approximation to solve the SDP, e.g., via Newton iterations applied to the KKT system, and "recenter" the computations at this new value.

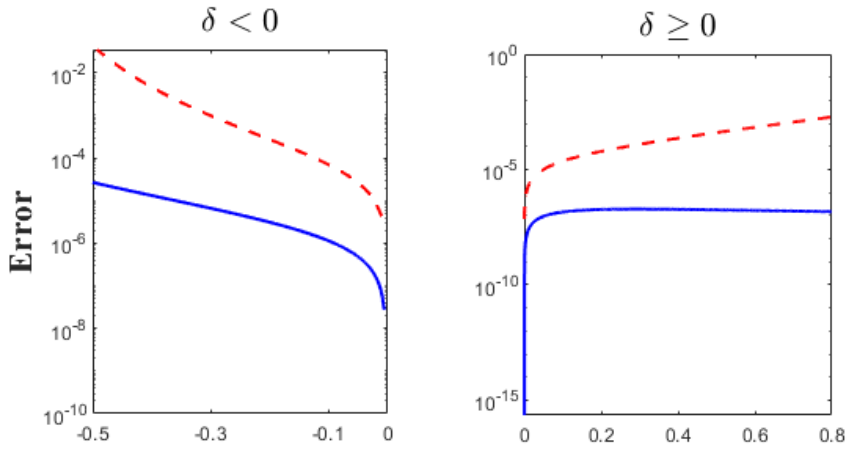

Figure 3: Plot of actual numerical error (solid) and upper bound of global error (dashed).

6.2. A two-parameter SDP with known non-convex MAPS

The previous example had a single perturbation parameter in which case the sweeping Euler scheme (SES) only "sweeps" in the positive and negative directions. In this section, we demonstrate the scheme on an example with two perturbation parameters. This parametric SDP is derived from a quadratic constrained linear program with a linear equality constraint and a quadratic inequality (the interior of circle), namely

$$\begin{array}{ll} \min & x_2 \\ \text{s.t.} & x_1 - \delta_1 x_2 = \delta_2 \\ & x_1^2 + x_2^2 \leq 1. \end{array}$$

Here δ_1 controls the slope of the linear constraint and δ_2 controls the y intercept. With no perturbation, i.e., $\boldsymbol{\delta} = 0$, the feasible set is the segment between -1 and 1 on y-axis within the unit circle. Let S^3_{ij} denote a symmetric matrix of size 3 with the $(i,j)^{\text{th}}$ and $(j,i)^{\text{th}}$ entry equal to one and zero elsewhere. The problem can be rewritten in standard format with the matrices in (1) and (2) defined as follows:

$$A_1 = S^3_{11}, A_2 = S^3_{22}, A_3 = S^3_{23}, A_4 = S^3_{33}, A_5 = S^3_{12}, C = S^3_{13}, D_1 = D_2 = 0, G = 0,$$
$$b = (1,1,0,1,0,0)^T, E_{15} = S^3_{13}, E_{25} = 2S^3_{11}, E_{ij} = 0 \text{ for } i = 1,2, \quad j = 1,\ldots,4.$$

It follows that the dual problem can be written as

$$\begin{aligned} \min \quad & y_1 + y_2 + y_4 \\ \text{s.t.} \quad & S = \begin{pmatrix} -2\delta_2 y_5 - y_1 & -y_5 & 1 - \delta_1 y_5 \\ -y_5 & -y_2 & -y_3 \\ 1 - \delta_1 y_5 & -y_3 & -y_4 \end{pmatrix} \\ & S \succeq 0 \end{aligned} \tag{25}$$

As δ_1 increases or decreases, the line governed by the linear constraint tilts right or left, respectively. Correspondingly, the range of δ_2 is determined by how far the line can be shifted while still intercepting with the unit circle, namely

$$\delta_1 \in \mathbb{R}, \quad \delta_2 \in \left(-\sqrt{1 + \delta_1^2}, \sqrt{1 + \delta_1^2} \right). \tag{26}$$

Given the bounded set $\delta_1 \times \delta_2 \in [-5, 5] \times [-5, 5]$, the comparison of numerical approximation of the maximum analytical perturbation set and the theoretical boundary is demonstrated in Figure 4. Notice that the SES recovers the MAPS with high accuracy even though the MAPS for this problem is non-convex. In general, this may not be true for the SES as the initial parameter point may not be connected via a straight line from the origin to every point to the true MAPS as explored in the examples below.

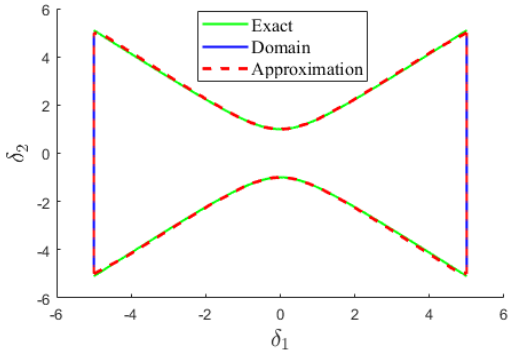

Figure 4: Comparison of the exact boundary and the approximation of the boundary using SES. The exact MAPS is described by the region enclosed by the solid green curves (described by Eq (6.2)) and two vertical blue lines (part of the bounded set). The numerical approximation is represented by the area enclosed by the red dash curves.

6.3. A three parameter SDP with known MAPS

Consider applying SES to the following three parameter SDP to show its performance on a problem with 3-D parameter space and *a priori* known non-convex MAPS:

$$\begin{aligned} \min \quad & \delta_1 x + (1 - \delta_1) y \\ \text{s.t.} \quad & \begin{pmatrix} 1 + \delta_2 & x & y & 0 & 0 \\ x & 1 & 0 & 0 & 0 \\ y & 0 & 1 & 0 & 0 \\ 0 & 0 & 0 & \frac{1}{2} + \delta_3 & x \\ 0 & 0 & 0 & x & \frac{1}{2} + \delta_3 \end{pmatrix} \succeq 0. \end{aligned} \tag{27}$$

The corresponding problem statement in the format of (1) includes 12 linear constraints with 12 A matrices of 5×5 among others, so we omit the expression of this problem in

the format of (1) or (2) for succinctness. The bounded set B is the unit sphere. This problem has regions of the MAPS which are not straight-line connected to the origin.

The parameter δ_1 determines the slope of the objective function, $\delta_2 + 1$ is the size of the circle which is part of the feasible set, and δ_3 determines the range of x, y value of the optimal solution which corresponding to the area between $[-\delta_3 - 1/2, \delta_3 + 1/2]$ within the circle controlled by δ_2. The analytic maximum perturbation boundary is described below using the following three cases.

$$\text{Case 1: for } \delta_2 \in (-1, \infty), \delta_3 \in \left(-\frac{1}{2}, \sqrt{\frac{1+\delta_2}{2}} - \frac{1}{2} \right),$$

$$\delta_1 \in \left(\frac{\delta_3 + \frac{1}{2}}{\delta_3 + \frac{1}{2} - \sqrt{1 + \delta_2 - (\delta_3 + \frac{1}{2})^2}}, \frac{\delta_3 + \frac{1}{2}}{\delta_3 + \frac{1}{2} + \sqrt{1 + \delta_2 - (\delta_3 + \frac{1}{2})^2}} \right);$$

$$\text{Case 2: for } \delta_2 \in (-1, \infty), \delta_3 \in \left(\sqrt{\frac{1+\delta_2}{2}} - \frac{1}{2}, \sqrt{1+\delta_2} - \frac{1}{2} \right),$$

$$\delta_1 \in \left(-\infty, \frac{\delta_3 + \frac{1}{2}}{\delta_3 + \frac{1}{2} + \sqrt{1 + \delta_2 - (\delta_3 + \frac{1}{2})^2}} \right);$$

$$\text{Case 3: for } \delta_2 \in (-1, \infty), \delta_3 \in \left(\sqrt{1+\delta_2} - \frac{1}{2}, \infty \right), \delta_1 \in (-\infty, 1).$$

For Case 1, the problem is feasible but the solution loses analyticity when passing through the boundary. In particular, the solution sheet of x, y become constant as shown in the bottom right corner figure of Figure 5. For Case 2, the optimal function value jumps along the upper bound as the slope of the objective function turns from negative to positive. For Case 3, solution is analytic within the unit sphere B.

Figure 5 shows the theoretical boundary and the numerical results for this example. The figure on the left shows the exact boundary surfaces which is described by the lower bound of Case 1 and upper bound of Cases 1 and 2. The blue surface is the numerical approximation using SES with the minimum eigenvalue threshold. As visible in the figure, the circular lines from the numerical approximation matches closely with the yellow surface from the exact boundary.

The right panel in Figure 5 shows the MAPS intersected with $\delta_2 = 0$. The exact MAPS is described by the upper boundary of in Case 1 and 2 and the unit circle which corresponds to the region enclosed by the black and blue solid line in the right figure. The numerical approximation is shown in red dash-dot line. The bottom right corner shows how the solution path of (x, y) change as δ_1 varies while $\delta_3 = 0$. It is clear that the solution path losses analyticity at critical point $\delta_1 = \frac{1}{1+\sqrt{3}}$.

A closer look at the top right corner of the left panel shows that there is some gap between the exact MAPS and the numerical approximation. The points within the gap are not straight-line connected to the origin. This observation implies that this gap will not be reduced even with high precision solutions of the PDE system. This issue can only be resolved by changing the initial solving point of the PDE system. We like to emphasize that the method presented here is the first step towards finding the true MAPS and the non-convex nature will be further investigated in future works.

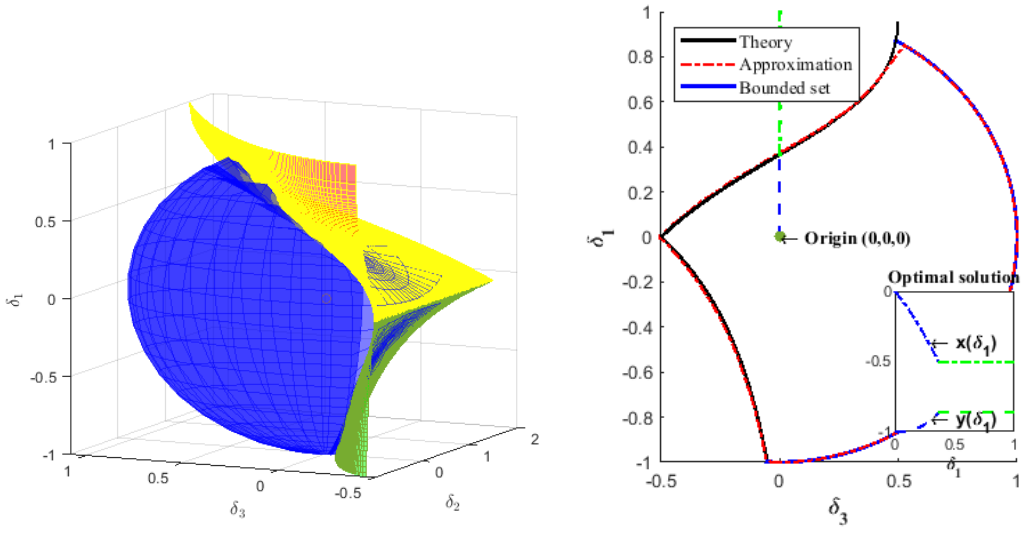

Figure 5: Left: Comparison of exact boundary and numerical approximation. Right: The comparison of exact boundary and numerical approximation at $\delta_2 = 0$. The green and blue dashed line represent the optimal solution path.

6.4. Comparison with SDP solvers: A two-parameter SDP with unknown MAPS

The previous examples all had analytical solutions and easily analyzed MAPS. To benchmark the performance of the SES for a generic problem with no *a priori* closed-form expression for the MAPS, we apply the scheme to an example S and X are 3×3 symmetric matrices with two perturbation parameters. For simplicity, we will only write the dual SDP (2), namely:

$$\begin{aligned}
\text{maximize} \quad & y_1 - 4y_2 \\
\text{s.t.} \quad & S_{.1} = \begin{bmatrix} \delta_1(-8y_1 - 4y_2 + 4) + \delta_2(10y_1 - 10y_2 + 6) - 2y_1 - 4y_2 - 8 \\ \delta_1(-6y_1 + 2y_2 + 5) + \delta_2(2y_1 + 9y_2 - 5) - 4y_1 + 6y_2 + 2 \\ \delta_1(-4y_1 + 5y_2 + 2) + \delta_2(-y_1 - 2y_2 + 6) + 9y_1 - 4y_2 + 8 \end{bmatrix} \\
& S_{.2} = \begin{bmatrix} \delta_1(-6y_1 + 2y_2 + 5) + \delta_2(2y_1 + 9y_2 - 5) - 4y_1 + 6y_2 + 2 \\ \delta_1(4y_1 + 6y_2 - 8) + \delta_2(10y_1 - 10y_2 - 6) - 10y_1 + 2 \\ \delta_1(-2y_1 - 9y_2) + \delta_2(4y_1 + 2y_2 - 3) + 6y_1 + 7y_2 + 6 \end{bmatrix} \\
& S_{.3} = \begin{bmatrix} \delta_1(-4y_1 + 5y_2 + 2) + \delta_2(-y_1 - 2y_2 + 6) - 9y_1 - 4y_2 + 8 \\ \delta_1(-2y_1 - 9y_2) + \delta_2(4y_1 + 2y_2 - 3) + 6y_1 + 7y_2 + 6 \\ \delta_1(-2y_1 - 6) + \delta_2(10y_1 - 8y_2 - 4) - 8y_1 - 4y_2 \end{bmatrix} \\
& S \succeq 0.
\end{aligned} \tag{28}$$

We first use SES to approximate the solution to problem (28) inside of the *a priori* unknown MAPS U within a ball of radius 3. Following Section 5, we first sweep using direction vectors

$$\boldsymbol{\alpha}(\theta) = \begin{pmatrix} \cos(\theta) \\ \sin(\theta) \end{pmatrix} \quad \text{for} \quad \theta \in [0, 2\pi).$$

Using an angular mesh step size of $\pi/180$, for each direction vector $\boldsymbol{\alpha}(\theta)$ selected, we start at the origin and solve the corresponding ODEs (12) along $\boldsymbol{\alpha}(\theta)$ with step size $1/1000$ until the derivative threshold criterion provides an approximation of the first

boundary of U in the direction of $\boldsymbol{\alpha}(\theta)$. In Figure 6, the left-hand side picture shows the approximation of the optimal value of the dual problem $m = y_1 - 4y_2$ in all directions, while the right-hand side picture is restricted to $\delta_1, \delta_2 \in [0, 0.05]$.

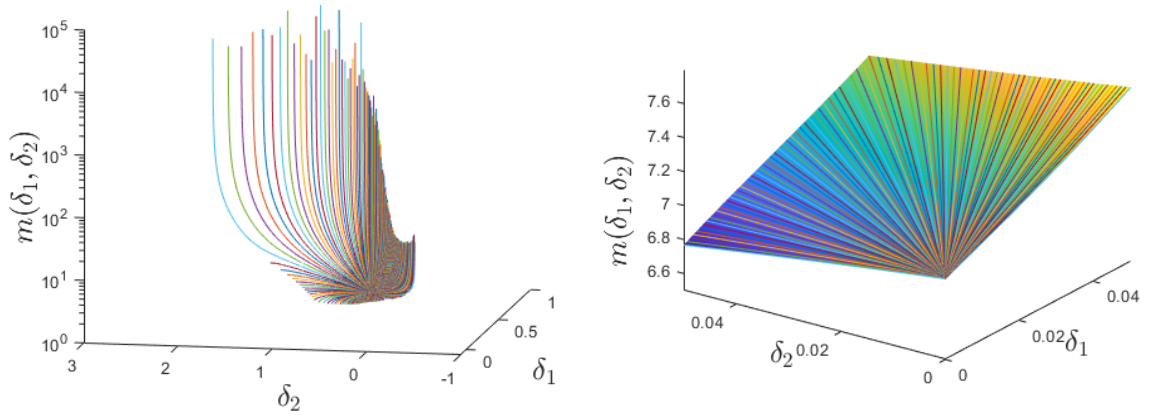

Figure 6: Plot of solution computing using SES in all directions (left) and on $[0, 0.05]^2$ (right).

There are several possibilities that create the boundary of U. First, the optimum of the SDP could become unbounded. This is observed in Figure 6 by the rays becoming nearly vertical at the boundary. Second, the optimum could become singular with respect to the KKT conditions. This could happen at the boundary between feasible and infeasible SDPs as well as having multiple solution sheets of the KKT system intersecting. A detailed classification of five different possible ways of losing analyticity along any given direction can be found in Bellon et al. (2021). The complete boundary of U is shown in the left panel of Figure 7.

Even though there are no other designated numerical methods that compute ∂U for parameteric SDPs, numerous generic SDP solvers such as CSDP, MOSEK, SeDuMi, SDPT3, DSDP, SDPA, and ADMM have been developed, e.g., see Mittelmann (2012); Wen et al. (2010), and these method can be used to find U by solving on the same meshgrid as the SES. One key difference is the SES utilize data from adjacent meshgrid points to update on the current point while the SDP solvers solve at each meshgrid point independently. This difference yields two advantages for SES: 1) it greatly speeds up the computational time and 2) it can capture all type of disruptions occurring in the optimal solution path as parameters change. In particular, the SDP solvers can only differentiate whether the parameteric SDP is solved or not, but cannot determine if the solution path is smooth which will cause failure in capturing ∂U. We compare the performance of SES with the SDP solver SDPT3 from Tütüncü et al. (2003). We chose SDPT3 due to its popularity in optimization modeling language, its advantages in solving small to medium scale SDP problems, e.g., see Mittelmann (2012); Tütüncü et al. (2003), and an easy-to-use interface via the MATLAB package CVX. In this comparison case, a boundary point is recorded whenever SDPT3 reports that the status is "not solved." Hence, equating "not solved" with infeasibility yields an outer approximation of ∂U. It is worth noting that one may have jumped over ∂U where the SDP is feasible an the solution lies on a different solution sheet while our SES approach identifies where such a switch occurs. In other words, the optimal solution path exists but not analytic anymore.

Our comparison utilized an angular mesh size of $\pi/180$ and step size of $1/1000$. The computational time and L_1 error of the approaches for $(\delta_1, \delta_2) \in [0, 0.05]^2$ are listed in

Table 2. It shows that our SES method is more than 100 times faster than using SDPT3 via CVX with comparable accuaracy in finding the optimal solutions.

Table 2: Comparison of CPU time (in seconds) and L_1 error.

Method	CPU time	L_1 error
SES	144.3	$1.07 \cdot 10^{-9}$
CVX-SDPT3	14,599.5	$2.00 \cdot 10^{-9}$

Figure 7(a) compares the boundaries computed using SES with SDPT3 via CVX. We observe that both provide an almost identical approximation of ∂U which reaffirms of the ability of SES in approximating ∂U. A discrepancy occurs for the angle $\theta = 249\pi/180$ (illustrated by the arrow in Figure 7(a)) where SES indicates a boundary near 0.169 units along this direction while the SDPT3 approach yields 0.204. The reason for this is illustrated in Figure 7(b) which shows a jump in the x_{11} coordinate between solution sheets for along the given direction at radius between 0.1690038 and 0.1690039. Thus, the optimum is not differentiable which is identified by our SES approach. By simply solving at mesh points, SDPT3 identified that the SDP had solutions on both sides of this so it continued to look for infeasibility which occurred much later. Therefore, the sensitivity of our SES approach combined with being two orders of magnitude faster with similar error show its dominance for computing ∂U over simply solving the SDP at mesh points looking for infeasibility.

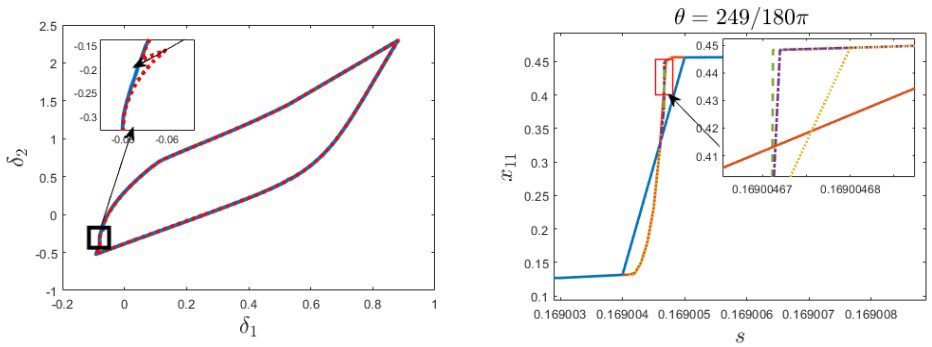

(a) (b)

Figure 7: (a): Comparion of ∂U for (28) using SES and a mesh solving approach using SDPT3 via CVX. The dashed line represents using SES while the solid line are the results from CVX-SDPT3 combination. (b): Demonstrating a jump in the value of x_{11}-coordinate of the optimum along the direction with angle $249\pi/180$ with four refined discretizations over radius.

6.5. Numerical approach for achieving high precision when approximating ∂U

Finally, we consider an approach to improve the approximation accuracy of the MAPS. For illustration, we consider an example with one parameter, namely:

$$\begin{aligned} \text{minimize} \quad & (1+2\delta)x_{11} - 2(1+\delta)x_{12} + (2+3\delta)x_{22} \\ \text{s.t.} \quad & (2+\delta)x_{11} + 2(3+2\delta)x_{12} + (1+3\delta)x_{22} = -1 \\ & X = \begin{bmatrix} x_{11} & x_{12} \\ x_{12} & x_{22} \end{bmatrix} \succeq 0, \end{aligned} \tag{29}$$

$$\begin{aligned} \text{maximize} \quad & y \\ \text{s.t.} \quad & S = \begin{bmatrix} 1+2y+\delta(2+y) & -1+3y+\delta(2y-1) \\ -1+3y+\delta(2y-1) & 2+y+\delta(3+3y) \end{bmatrix} \succeq 0. \end{aligned}$$

The analytic expression of the optimal dual solution for y is

$$y = \frac{13\delta^2 + 19\delta + 9 + \sqrt{189\delta^4 + 654\delta^3 + 959\delta^2 + 590\delta + 125}}{2(\delta^2 + 7\delta + 11)}. \tag{30}$$

The lower bound of the MAPS occurs at the largest negative root of quartic polynomial under square root in (30), namely

$$\delta_c = \frac{a_3 - 109}{126} + \frac{1}{2}\sqrt{\frac{239104}{3969a_3} - \frac{1030}{1323} - \frac{a_1 + a_2}{567}} \approx -0.49347124103$$

where

$$a_1 = \sqrt[3]{11113649 + 34560\sqrt{24019}}, \quad a_2 = \sqrt[3]{11113649 - 34560\sqrt{24019}}, \quad \text{and} \quad a_3 = \sqrt{7(a_1 + a_2) - 1545}.$$

We first compare approximating the corresponding boundary point using the eigenvalue and derivative threshold criteria described in Section 5 starting from $\delta = 0$. To this end, Table 6.5 compares using different step sizes with different threshold values C_1 and C_2, respectively. In both cases, the best one can hope for is to compute δ_c with an error bounded by the step size. This table shows that this is precisely the case for the derivative threshold criterion. In particular, the derivative threshold criterion is more stable than the eigenvalue threshold criterion for approximating the boundary starting at $\delta = 0$.

Table 3: Comparison of eigenvalue and derivative threshold for approximating the boundary.

	Eigenvalue threshold C_1			Derivative threshold C_2		
Step size	-10^{-5}	-10^{-4}	-10^{-3}	0.1	1	10
1/10	−0.5	−0.5	−0.5	−0.5	−0.5	−0.5
1/100	−0.33	−0.44	−0.49	−0.49	−0.50	−0.50
1/1000	−0.475	−0.490	−0.494	−0.493	−0.493	−0.494

Since these criterion can only approximate the boundary up to the step size, it could be computationally expensive to produce highly accurate approximations by simply reducing the step size. One may also appeal to Proposition 1 and Corollary 1 to construct algebraic conditions that vanish on the boundary. The approach considered here is based on a modification of the endgame described in Morgan et al. (1992). In particular, we aim to to compute the unknown boundary point δ_c by constructing a Puiseux series centered at δ_c. For singularities of multiplicity 2, which is the generic case described in Dedieu and Shub (2001), we can build a Puiseux series with half powers of the form

$$m(\delta) = \sum_{j=0}^{\infty} c_j(\delta - \delta_c)^{\frac{j}{2}}$$

which, for some constants $c_j \in \mathbb{R}$, holds for δ near δ_c. Using n data points, say $(\delta_j, m(\delta_j))$ for $j = 0, \ldots, n-1$, one can simultaneously approximate the boundary point δ_c and the first $n-1$ coefficients $c_0 = m(\delta_c), c_1, \ldots, c_{n-2}$ using interpolation. Table 4 compares using two different step sizes $\Delta\delta$, namely 1/100 and 1/1000, with three choices of n, namely $3, 5, 7$, with the actual values. In this table, we list δ_0 with $\delta_j = \delta_0 - j\Delta\delta$

for $j = 1, \ldots, n-1$. The values are presented up to the first incorrect digit with the correct digits highlighted in red. In particular, we see that just with the knowledge of the boundary to 3 digits of accuracy, the Puiseux series interpolation can quickly be used to approximate the boundary value with 7 digits of accuracy. One could continue to play this modification of the endgame of Morgan et al. (1992) to compute the boundary point as accurately as required.

Table 4: Comparison of using Puisuex series to approximate boundary point.

Step size	δ_0	n	Approximation of δ_c	Approximation of $c_0 = m(\delta_c)$
1/100	-0.49	3	-0.498	0.14
		5	-0.4933	0.18
		7	-0.49349	0.178
1/1000	-0.493	3	-0.4935	0.177
		5	-0.49347121	0.1790763
		7	-0.49347125	0.179075
Actual values			-0.493471241	0.17907623

7. Conclusion and remarks

In this paper, we developed an algorithm to compute the maximal analytical perturbation set (MAPS) for a parametric SDP. The problem of solving semidefinite programs (SDPs) under affine perturbations in both primal and dual feasible sets is reformulated as solving a system of quasilinear partial differential equations (PDEs). A second-order sweeping Euler scheme (SES) is developed to solve the system of quasilinear PDEs which is well-posed on the interior of the MAPS.

There are three main computational challenges for computing the MAPS U: non-convexity of U, exponential computation time with respect to the dimension of perturbations, and the uniform precision for approximating U. We demonstrate the performance the SES method on several examples with non-convex MAPS. There are cases when the parameter corresponding to the initial SDP with no perturbations is straight-line connected to all points in the MAPS as in Example 6.2. However, in general, straight-line connections from the origin will not yield the entire MAPS. One possible solution is using a random spiral search algorithm or random restarts from other points in the MAPS. As for the computational time cost, we like to point out that, given the PDE system in Theorem 4, the SES algorithm can be vectorized to compute all direction at the same time. In addition, the SES algorithm can be modified to utilize state-of-art GPUs as the core computation involving large matrix operations. Finally, we presented different approaches of addressing the need of high accuracy in approximating the boundary of U.

We also compared our SES method with existing SDP solvers using SDPT3 by Tütüncü et al. (2003) via CVX in MATLAB and a finite difference scheme (FDS) on a family of SDPs parameterized by two affine perturbations. The data shows that the SES is clearly advantageous over the other two methods. In addition, SES only requires one point while the FDS requires additional boundary conditions.

Finally, we note that this method is not limited to just affine perturbations. In fact, both the theory and numerical computations needs for the SES method naturally extend to SDPs with sufficiently smooth nonlinear perturbations.

References

Ackleh, A.S., Allen, E.J., Kearfott, R.B., Seshaiyer, P., 2009. Classical and Modern Numerical Analysis: Theory, Methods and Practice. Taylor and Francis Publishing.

Alizadeh, F., Haeberly, J.P.A., Overton., M.L., 1998. Primal-dual interior-point methods for semidefinite programming: convergence rates, stability and numerical results. SIAM Journal on Optimization 8, 746–768.

Bellon, A., Henrion, D., Kungurtsev, V., Mareček, J., 2021. Time-varying semidefinite programming: Geometry of the trajectory of solutions. arXiv:2104.05445.

Ben-Tal, A., El Ghaoui, L., Nemirovski, A., 1998. Robust semidefinite programming. Handbook on Semidefinite Programming 27.

Blekherman, G., Parrilo, P.A., Thomas, R.R., 2012. Semidefinite optimization and convex algebraic geometry. SIAM.

Causon, D.M., Mingham, C.G., 2010. Introductory finite difference methods for PDEs. Bookboon.

Dedieu, J.P., Shub, M., 2001. On simple double zeros and badly conditioned zeros of analytic functions of n variables. Mathematics of Computation , 319–327.

EL Ghaoui, L., Oustry, F., Lebret, H., 1998. Robust solutions to uncertain semidefinite programs. SIAM Journal on Optimization 9, 33–52.

Evans, L.C., 2010. Partial Differential Equations–second edition, volume 19 of Graduate Studies in Mathematics. American Mathematical Society, Providence, RI.

Goldfarb, D., Scheinberg, K., 1999. On parametric semidefinite programming. Applied Numerical Mathematics 29, 361–377.

Haeberly, J.P., 1998. Remarks on nondegeneracy in mixed semidefinite-quadratic programming. Technical Report, Department of Mathematics, Fordham University.

Hao, W., Hauenstein, J.D., Hu, B., Sommese, A.J., 2011. A three-dimensional steady-state tumor system. Applied Mathematics and Computation 218, 2661–2669.

Harrington, H.A., Mehta, D., Byrne, H.M., Hauenstein, J.D., 2020. Decomposing the parameter space of biological networks via a numerical discriminant approach, in: Gerhard, J., Kotsireas, I. (Eds.), Maple in Mathematics Education and Research, Springer International Publishing, Cham. pp. 114–131.

Hauenstein, J.D., Mohammad-Nezhad, A., Tang, T., Terlaky, T., 2022. On computing the nonlinearity interval in parametric semidefinite optimization. Mathematics of Operations Research 47, 2989–3009.

Kalaba, R.E., Zagustin, E., Holbrow, W., Huss, R., 1977. A modification of Davidenko's method for nonlinear systems. Computers & Mathematics with Applications 3, 315–319.

de Klerk, E., 2006. Aspects of Semidefinite Programming: Interior Point Algorithms and Selected Applications. volume 65 of Series Applied Optimization. Springer.

Miller, S.A., 1997. Sensitivity of solutions to semidefinite programs. Center for Control Engineering and Computation. University of California at Santa Barbara, Tech. Rep. CCEC-97-0519.

Mittelmann, H.D., 2012. The state-of-the-art in conic optimization software, in: Handbook on Semidefinite, Conic and Polynomial Optimization. Springer, pp. 671–686.

Moerdijk, I., Reyes, G.E., 1991. Models for smooth infinitesimal analysis. Springer-Verlag, New York.

Morgan, A.P., Sommese, A.J., Wampler, C.W., 1992. A power series method for computing singular solutions to nonlinear analytic systems. Numerische Mathematik 63, 391–409.

Piret, K., Verschelde, J., 2010. Sweeping algebraic curves for singular solutions. J. Comput. Appl. Math. 234, 1228–1237.

Sard, A., 1942. The measure of the critical values of differentiable maps. Bulletin of the American Mathematical Society 48, 883–890.

Sekiguchi, Y., Waki, H., 2021. Perturbation analysis of singular semidefinite programs and its applications to control problems. Journal of Optimization Theory and Applications 188, 52–72.

Todd, M.J., Toh, K.C., Tütüncü, R.H., 1998. On the nesterov–todd direction in semidefinite programming. SIAM Journal on Optimization 8, 769–796.

Tütüncü, R.H., Toh, K.C., Todd, M.J., 2003. Solving semidefinite-quadratic-linear programs using sdpt3. Mathematical Programming 95, 189–217.

Wen, Z., Goldfarb, D., Yin, W., 2010. Alternating direction augmented lagrangian methods for semidefinite programming. Mathematical Programming Computation 2, 203–230.